Muon flux measurement

Alberto Appoloni, Massimo Fellin, Andrea Pegoretti, Nicolò Russo, Erika Socal

Contents

Chapter 1

Introduction

The aim of the experience in the laboratory is to detect and analyze the muon flux produced by the interaction of cosmic rays with the upper layer of the atmosphere.
The parameters obtained with the procedure of data acquisition and analysis are:

- The size of the flux,
- The direction of the motion (whether they come from above or below),
- The mean velocity of the particles.

1.1 Experimental setup

The apparatus of the experiment consists in four NaI(Tl) scintillator layers placed in pairs on the top and the bottom of the room (at a distance of approximately $369m$ between 02 and 13), isolated from external disturbances with the help of black papers and tape strips. A scintillator converts the energy released by the charged particle ionizing the crystal into characteristic photons.
The NaI(Tl) is the most efficient inorganic scintillator in terms of light yield, while the typical timing (τ) for the rising tail of the signal is intermediate compared to other inorganic devices. Its general properties are summarized in Table 1.1.

$\tau\ [ns]$	230
$\lambda\,[nm]$	415
light yield	$40k\gamma/MeV$

Table 1.1: NaI(Tl) characteristics.

The emission wavelength correspond to the highest quantum efficiency for alkali-photocathodes. The light emitted by the scintillators is collected by means of WLS fibers to optimize the coupling with the following stage, the PMT.

A photomultiplier tube transforms the light entering the cathode into an electron cascade, transforming even the weakest signal into a detectable output. The most significant property is the linearity of the process, which allows to reconstruct the initial energy deposited. The dinodes are powered by high voltage and low current, this lead to the need of use of SHV cables.

The four signals are transferred with BNC cables from the PMT to the FAN-IN FAN-OUT, that allows to electronically split them without using physical objects. This procedure is important to avoid undesired reflection of the wave and half the signal amplitude. One of the FAN-IN FAN-OUT outputs goes as an input for the AND port to check for the coincidence, after this step the result is sent to the digitizer as a trigger; the other splitted signal goes directly to the relative channel of the digitizer that automatically records the value of the voltage on each of the 1024 capacitors every $200ps$.

When the coincidence turns on the trigger, the signal stored on the capacities for the previous $1024 \times 0.2ns = 204ns$ is saved in an ASCII file and can be used later on for the analysis. If the trigger does not open the recording procedure, the capacities are overwritten and the previous data are deleted. This method allows to reconstruct the shape of the signal related to the energy released by the muons in the scintillator, only when coincidence occurs.

From the waveform through data analysis it is possible to extract the time when the muon crosses the scintillator, this is done with the aim of deriving the β knowing the distance travelled.

The impedance of the digitizer is set at 50Ω, to match the ideal value carried by the coaxial cables transporting the signal.

An additional check for the velocity is provided by a Čerenkov detector placed right above the two lower scintillators. This is connected to a PMT (here called PMT1) which produces a measurable signal of the Čerenkov radiation. Right above the bulk, a scintillator is placed equipped with other two PMTs (here called PMT2 and PMT3). PMT2 lies in a perfect vertical line with PMT1, as its aim is to reject muons which cross both.

The reason for the introduction of this detector relies in the number of Čerenkov photons, that is proportional to the velocity of the relativistic particle, evaluated with highest resolution compared to ToF.

The data analysis of this second device is not carried out in this work.

Chapter 2

Data analysis and discussion

2.1 Preliminary steps

2.1.1 Evaluation of the intrinsic delay

The first step is the evaluation of the noise source due to the delay of the cables.
For this procedure the scintillator plates are disassembled from their running positions and fixed in a support that permits to flip the order of the layers upside down. Thanks to this method, this delay is mathematically evaluated as a mean between the time of flight recorded by the instrumentation in the right configuration and in the flipped one, ΔT and ΔT^F:

$$\tau = (T_{c3} - T_{cX}) = \frac{\Delta T + \Delta T^F}{2} \tag{2.1}$$

where T_{c3} is the reference cable time delay and T_{cX} is the one given by the X scintillator, with $X = 0, 1, 2$. ΔT and ΔT^F experimentally represent the mean value of the bell-shaped behaviour clearly visible in Figures 2.1 ad 2.2 below. Equation 2.2 shows the delay and the error evaluated from the Gaussian fit.

$$T_1 \pm \sigma_{T_1} = (0.44 \pm 0.02)ns \qquad T_2 \pm \sigma_{T_2} = (2.97 \pm 0.02)ns \tag{2.2}$$

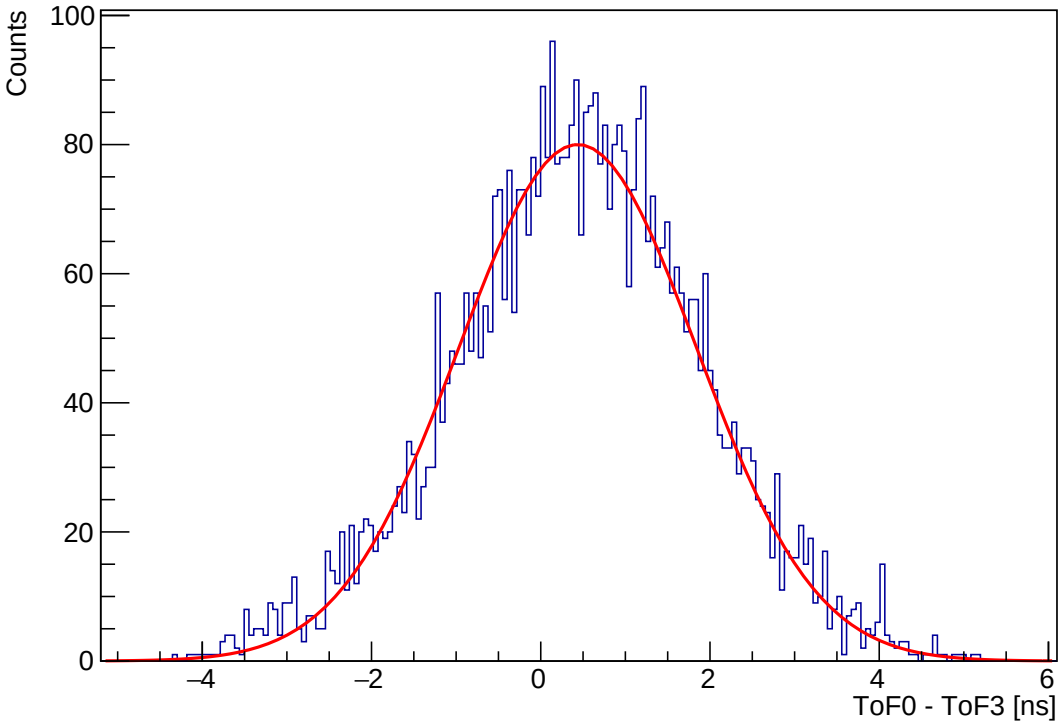

Figure 2.1: Delay of the cable 1 with respect to the reference, cable 3, in the right configuration.

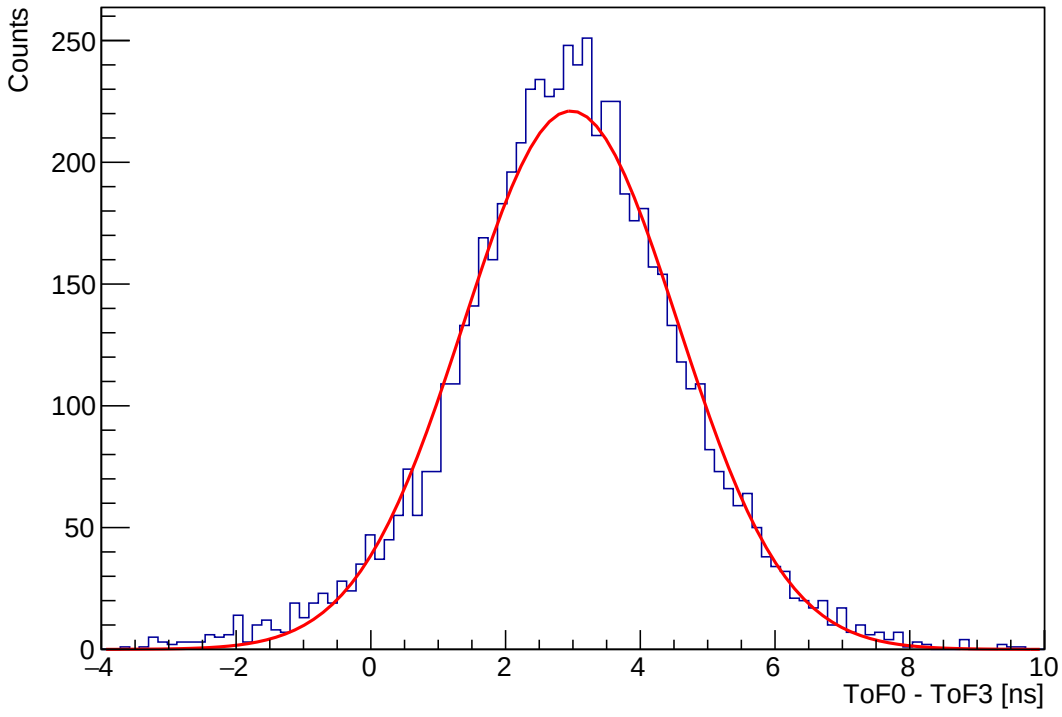

Figure 2.2: Delay of the cable 1 with respect to the reference, cable 3, in the flipped configuration.

Finally, the value of this delay can be found by simply applying Equation 2.1 between the two

peaks, with error given by the propagation. This procedure is done for all the combinations possible: ToF3-ToF0, ToF3-ToF1, ToF3-ToF2, and the results are presented in Table 2.1.

ToF3-ToF0	$(1.71 \pm 0.02)ns$
ToF3-ToF1	$(3.05 \pm 0.02)ns$
ToF3-ToF2	$(0.88 \pm 0.01)ns$

Table 2.1: Single value of time delay for each combination of scintillators.

The τ must be added to all the TOF signal coming from the scintillators number 0, 1 and 2, while the number 3 is taken as a reference and it is supposed to have zero delay.
The Figures 2.3 and 2.4 plots the signals before and after the temporal translation for the 03 channels.

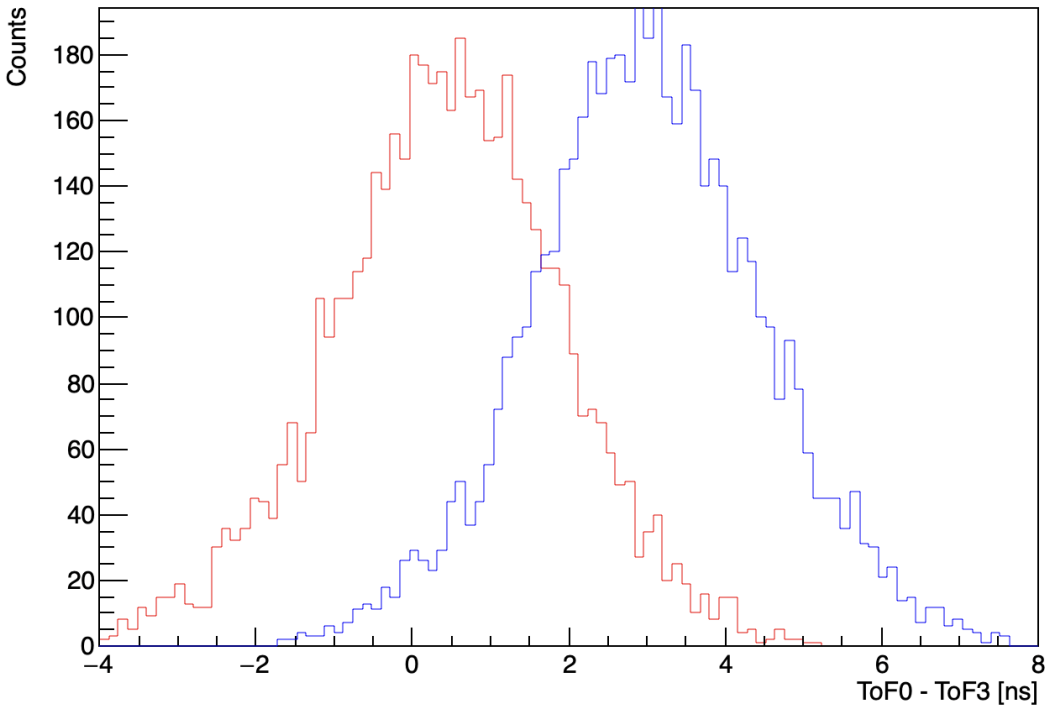

Figure 2.3: Pre cable-delay correction 03.

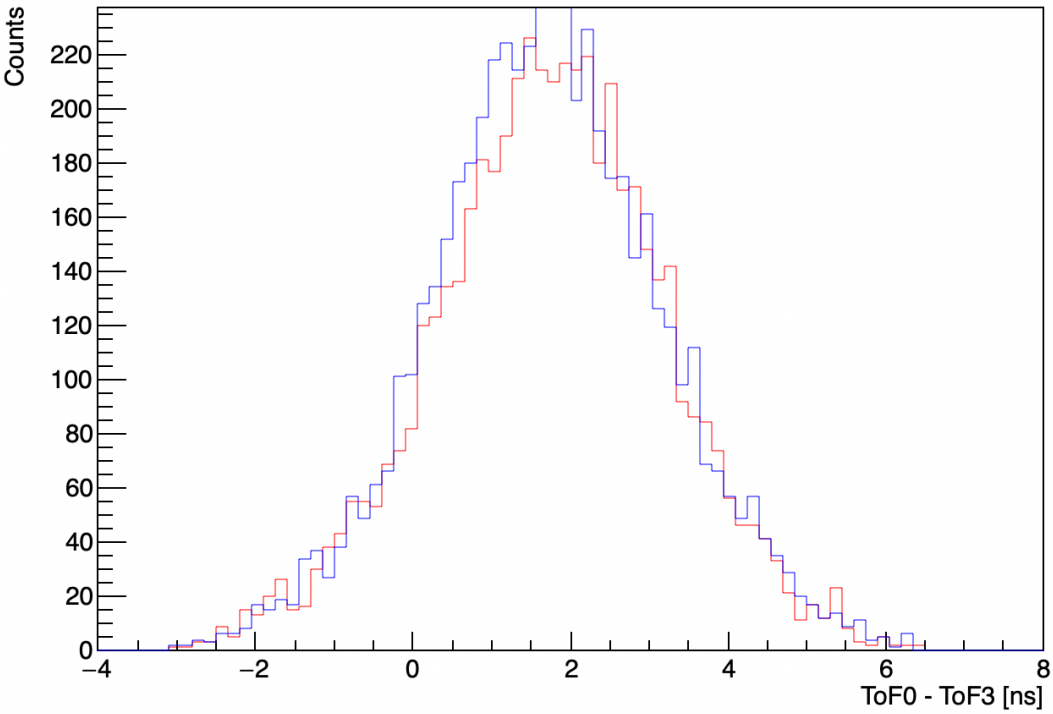

Figure 2.4: Post cable-delay correction 03.

2.1.2 Check for the inclination dependence

As an additional exercise, few data are taken with a progressively high inclination of the support, allowing to check the muon flux dependence on the azimuthal angle of incidence. The number of events are taken connecting the exit of the AND logic port (working in coincidence) to the counter of the CAEN module. The expression known *a priori* states that the proportionality between the recorded flux and the reference vertical muon flux relies in the $\cos^2\theta$, that can be easily found from our data available:

$$\cos^2\theta = 1 - \sin^2\theta = 1 - \left(\frac{h}{0.52}\right)^2 \tag{2.3}$$

where h is the height of the vertex and $0.52m$ is the hypotenuse, i.e. the basement of the support.

Table 2.2 summarizes the number of events recorded per each run at different inclinations, while Figure 2.5 highlights the linear relation. The straight line plotted is considered as follows:

$$y = ax + b \tag{2.4}$$

$\cos^2\theta$	time(s)	number of events
1	120	664
0.9	141	700
0.35	392	700
0	981	534
1^*	120	739

Table 2.2: Flux of muons in terms of the angle. 1^* refers to the flipped configuration.

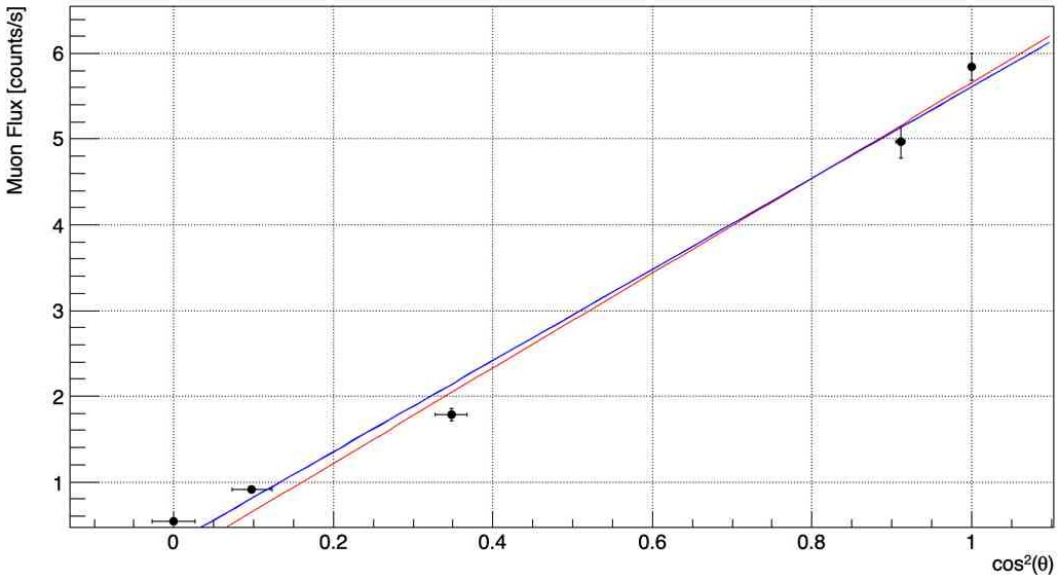

Figure 2.5: Behaviour of the flux with the azimuthal angle of inclination of the apparatus. The dots represent the experimental data with their relative errors. The blue line is the linear fit evaluated considering all the points, while the red line is the linear fit computed excluding the 0 value for a better estimation, as at $\theta = 90°$ the detector has an higher acceptance and the point suffers a bias.

In Figure 2.5 the experimental error for the flux is estimate with the square root of the counts, as the process is considered to be a Poissonian, while for the angle a propagation is performed considering the expression in Equation 2.3 used to found $\cos^2\theta$, and evaluating the error of each length measurement with $0.5mm$.
The results of this linear fit are presented in Tables 2.3 and 2.4.

a	5.3±0.2
b	0.3±0.1
χ^2	14.6
d.o.f	3

Table 2.3: Blue linear fit considering the value in zero.

a	5.5±0.2
b	0.11±0.13
χ^2	9.6
d.o.f	2

Table 2.4: Red linear fit excluding the value in zero.

An important note must be said, namely that the counter might consider a single muon as two distinct event. This is because the signal can drop again under the threshold after the signal rising relaxation, opening another coincidence gate.

2.1.3 Evaluation of the baseline

In order to evaluate the energy of an event, the area of the signal is the fundamental parameter. For this reason the evaluation of the baseline for each event is crucial, as it represent the upper threshold of the dropping signal.
Consider Figure 2.6 as an example of muon track. The procedure starts with the arithmetic mean and standard deviation of the first 20 points, let us call it $\overline{m}$ and σ, this is because for sure the first points belong to the baseline. An error σ_i is associated to each of the following points belonging to the waveform d_i, evaluated considering the distance from $\overline{m}$:

$$\sigma_i = |\overline{m} - d_i| + \sigma \tag{2.5}$$

After this operation, a linear fit is performed with all the points of the dataset, giving the intercept and the slope of the baseline. Points with large error (the deepest in the signal that are more distant from $\overline{m}$) will account less in the fit, in such a way only the points that are effectively on the baseline are considered. The great advantage of this method is that in the data analysis we don't have to cut the points where the waveform falls, which varies in time window between each acquisition.
This method is applied to all the dataset.

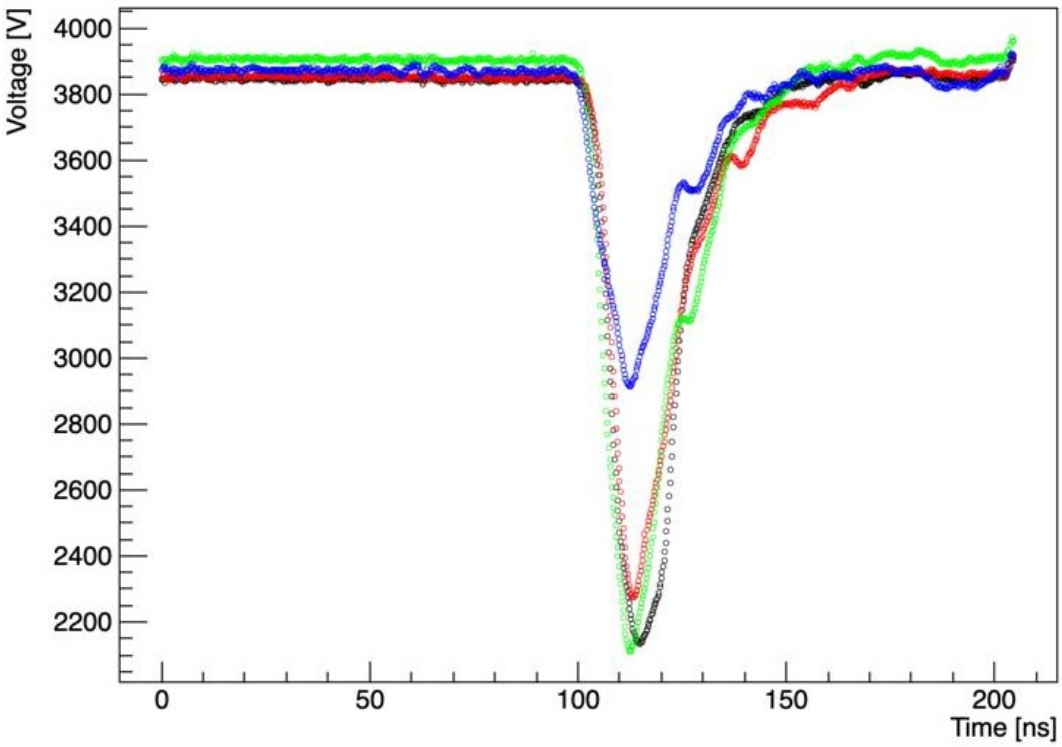

Figure 2.6: Example of muon signal.

2.2 Data rejection

The data acquisition where performed over three separated runs, spanning a total time of about two weeks. This allows to accumulate enough waveforms to built a sufficiently strong statistics in the analysis.
Through a specific C++/ROOT program, each coincidence can be reconstructed and analyzed to extract:

- the linear fit of the baseline
- the minimum depth of the signal and the maximum which should correspond to the baseline
- the time of arrival of the muon, considered as the time at half the signal depth
- the area of the whole signal with respect to the baseline fit
- the absolute area without the baseline reference

Among all the data acquired, a large fraction must be rejected as bad muon signals. The characteristics to be investigate are shown in the following and all concern a ToF rejection.

2.2.1 Saturation

The first data to be eliminated are those related to the saturation of the detector, since it is impossible to evaluate correctly the time-at-half-height.
Saturation implies same drop of the signal (constant baseline-minimum distance) but different energy released, evaluated as area with respect to the baseline. Since the energy released and the minimum of the signal are proportional in condition of no saturation, a linear fit is performed in the first proportional region, excluding all data that are not contained within a proper window near this line.

2.2.2 Short timing rejection

The second cut consists in the rejection of the data that show an anomalous behaviour in terms of timing in scintillator crossing: some events are recorded to hit first the lower scintillator and then the upper one in the closest couple, placed above the roof and under the floor; additionally, other muons take an anomalously large time to cross them.
In this perspective, the time difference between scintillators 02 (*invbeta02*) and 13 (*invbeta13*), normalized to the distance to get $\frac{1}{\beta}$, has been plotted in a 2D histogram. In Figure 2.8 an example is shown, considering $\frac{1}{\beta}$ and the time to cross the first couple of detector, 01. On the x axis the time required to cross the two closest scintillators is present, while on the y axis the respective inverse β.
The cutting procedure, as can be seen from Figure 2.8, consists in the elimination of the points outside the main region with respect to the x axis (time taken to fly from scintillators 01 in this particular case). Indeed, this method does not allow to eliminate all the superluminar events in the y axis, since those appear to have the correct timing response.

2.2.3 Comparison of ToF 02 and ToF 13

To perform a ToF analysis only one couple of scintillator is sufficient. The overabundant number of scintillators allows to further discriminate good data by comparing the results obtained from the ToF 02 and ToF 13: the mean and the difference event per event is performed and plotted in Figure 2.9.
Since the two scintillators are supposed to measure the same muon, in principle they should reproduce a $\Delta\beta = 0$. To tolerate statistical fluctuations, a large window centered in this value is applied to accept data, allowing for additional cut of too slow or too fast muons.

2.2.4 Conditioning

The whole dataset for one of the three runs is presented in Figure 2.10, before every rejection previously described: a 2D histogram with in the y axis *invbeta02* and in the x axis *invbeta13*. In principle we would expect an isotropic circular area while an elliptical area is observed. This points out that a conditioning is present in our acquisition: when a couple measure a slow muon, the other one record the same event as superluminar, and *vice versa*. This can be explained looking at the setup, since the scintillators present the PMT in different locations, the light collection takes different times and affects the measurements.

2.2.5 Time over Threshold

In Figure 2.11 the number of points below $500V$ from the baseline versus the drop has been plotted in a 2D histogram for the 0 scintillator. The number of points below a certain threshold is a key parameter when dealing with saturation since, even though the minimum saturates, the shape of the signal will be different depending on the energy released.
In Figure 2.11 it is possible to identify three regions: the first one below $500V$, where no points have been registered since the signal is not enough deep, the second where saturation has not occurred, and a third region of saturation where, even if the depth of the signal does not change, the number of points below threshold changes proportionally to the energy released in the scintillator. It can be seen that the non saturation region exhibits a logarithmic-like behaviour. Even if at first sight could appear anomalous, this trend can be explained remembering that the rising part of the signal dominates, in terms of points number, the time over threshold (compared to the drop part of the signal) and has an exponential-like behaviour.

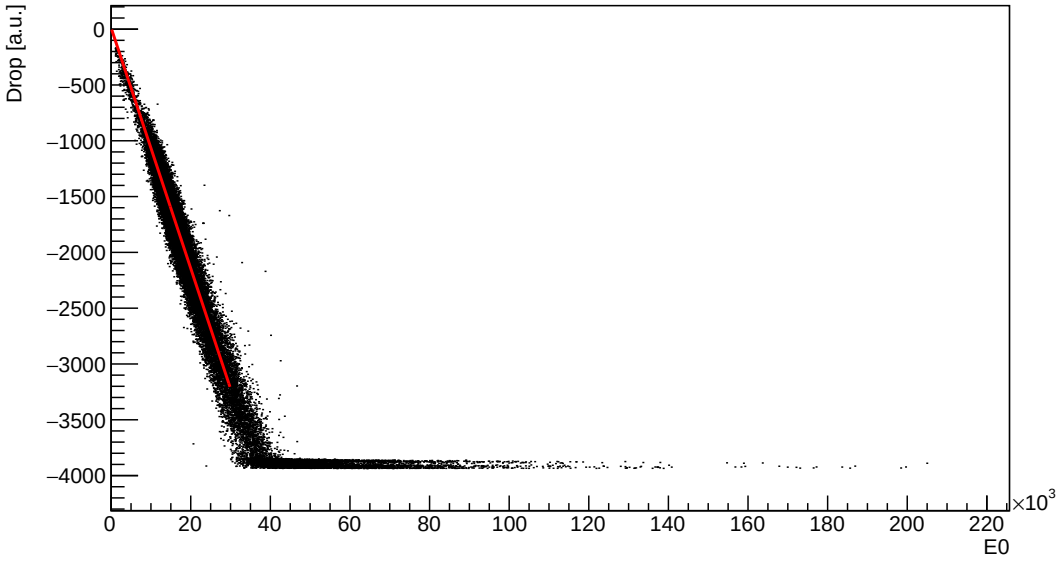

Figure 2.7: Muon saturation signal.

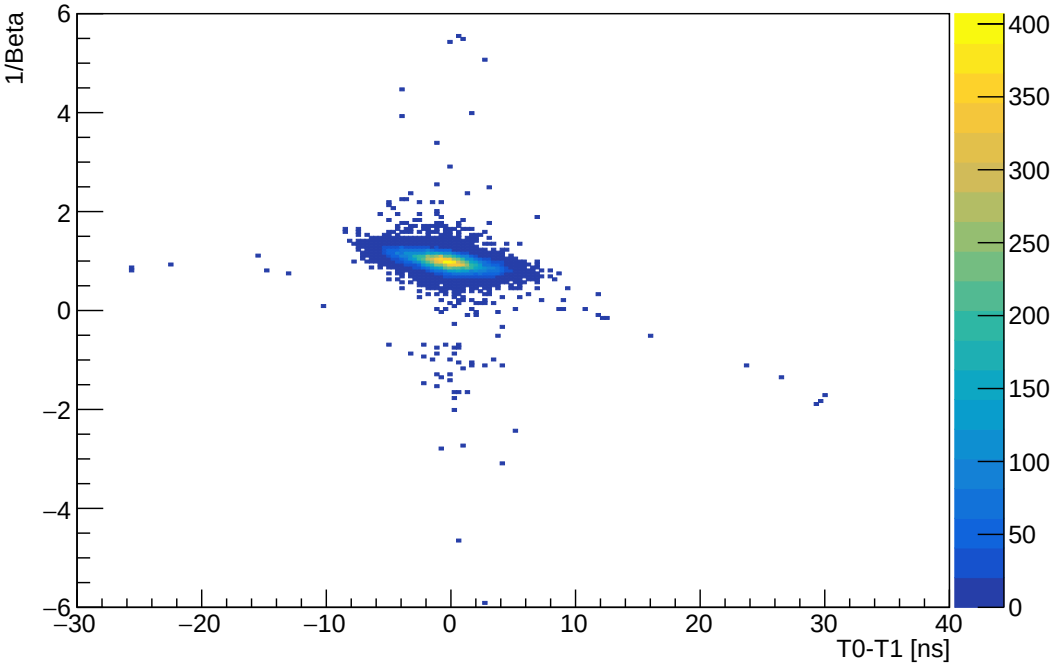

Figure 2.8: Histogram of the inverse velocity of all the events in a single run.

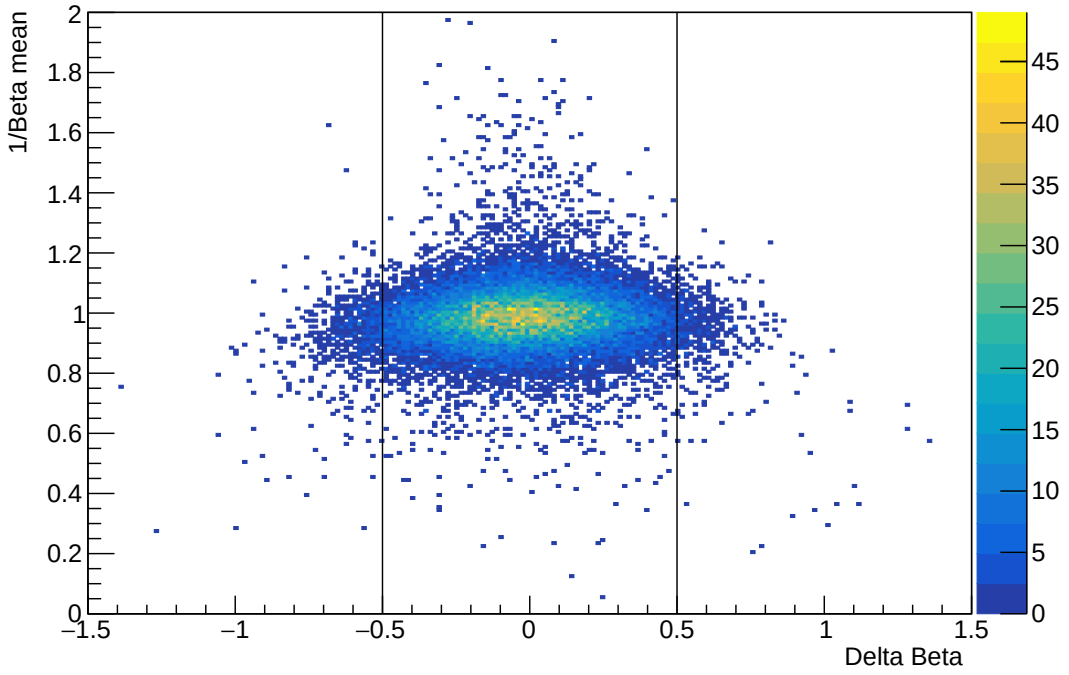

Figure 2.9: Plot of the mean value of $\frac{1}{\beta}$ between the two couple of scintillators with respect to the difference of the same parameter.

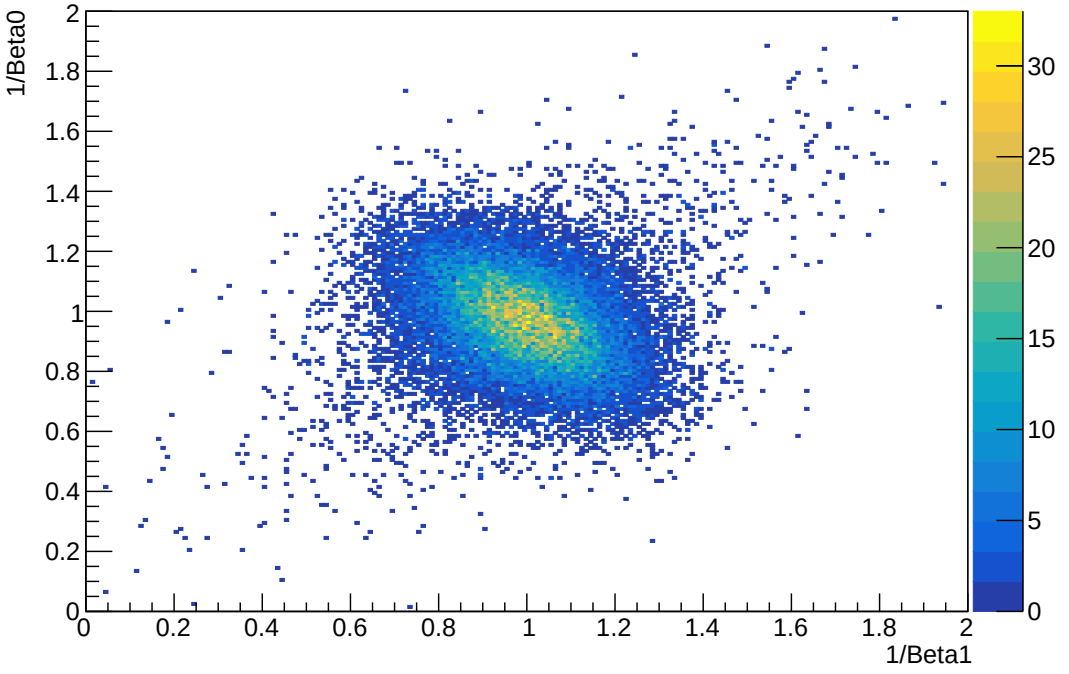

Figure 2.10: Graph of the inverse β parameter for the two couple of scintillators. The observed elliptical pattern suggests a conditioned experiment.

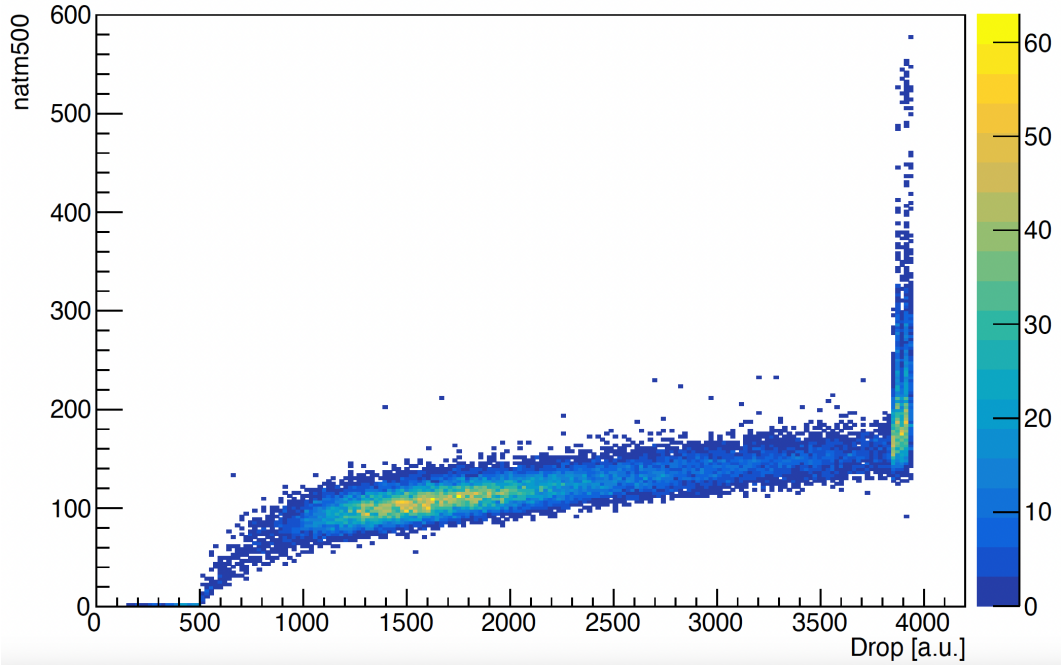

Figure 2.11: Time-over-threshold for scintillator 0.

2.3 Results

In this section, the final results for the velocity of the muons are reported.

Three runs, each lasting several days to get enough statistics, have been carried out. In Figure 2.12 the histogram of the value of $\frac{1}{\beta}$ acquired from scintillators 02 is presented, while for the couple 13 Figure 2.13 follows (both presented after proper data rejection).

RUN	β
1	1.023 ± 0.003
2	1.030 ± 0.003
3	1.028 ± 0.003
mean	1.027 ± 0.002

Table 2.5: Results for ToF 02.

RUN	β
1	1.007 ± 0.003
2	1.016 ± 0.003
3	1.008 ± 0.003
mean	1.010 ± 0.002

Table 2.6: Results for ToF 13.

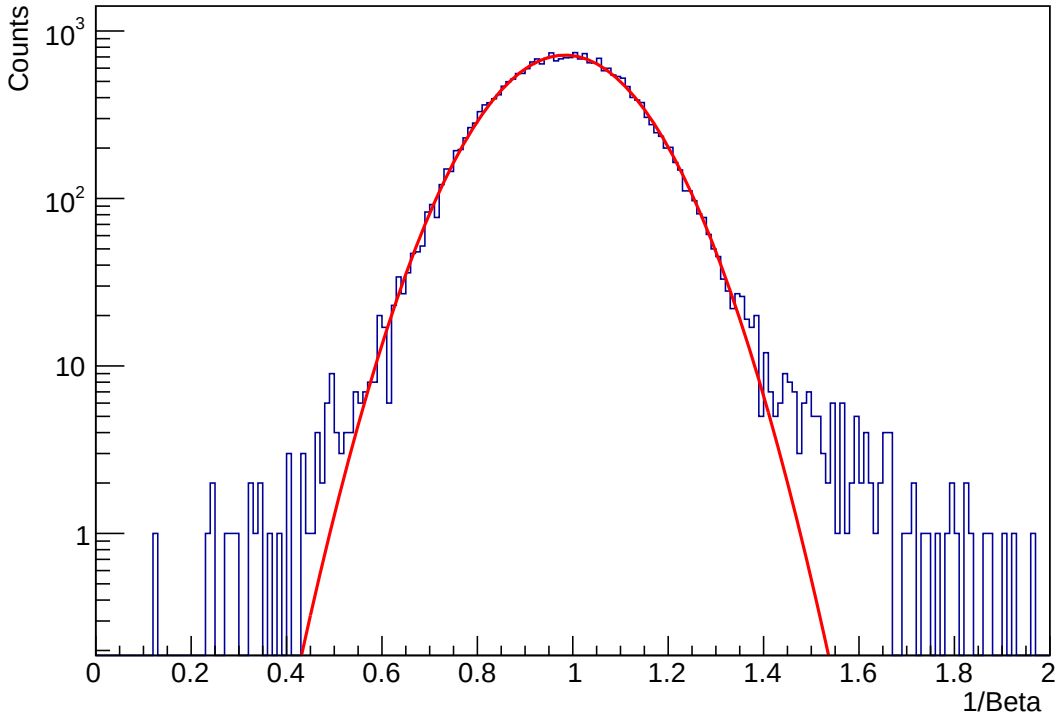

Figure 2.12: $\frac{1}{\beta}$ result from ToF 02.

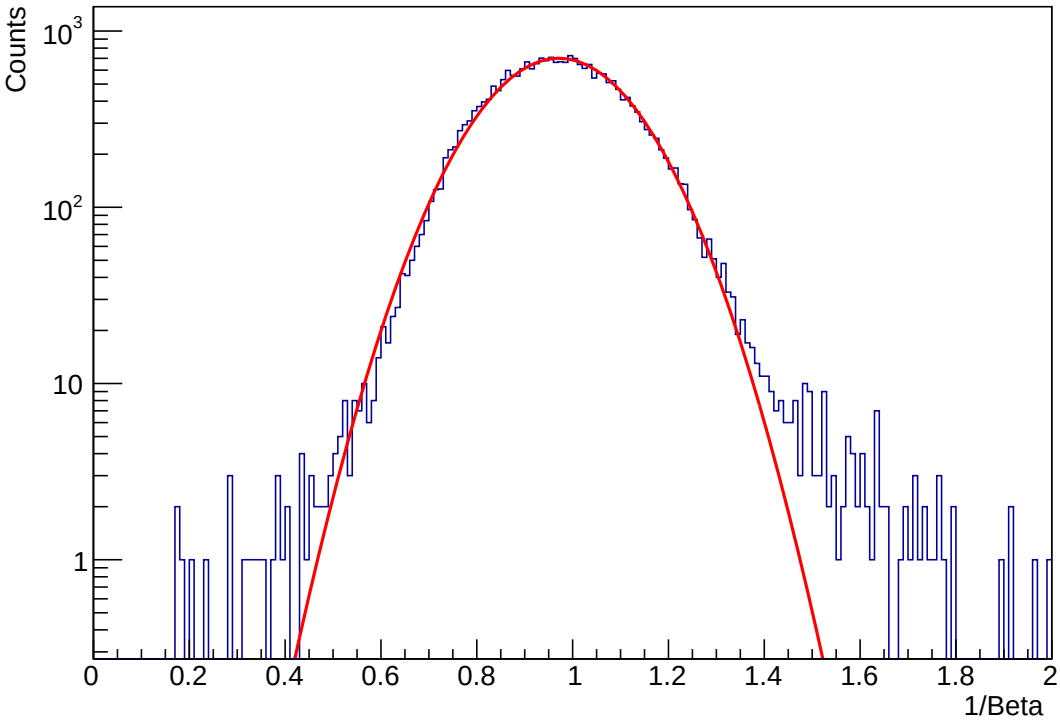

Figure 2.13: $\frac{1}{\beta}$ result from ToF 02.

As can be seen from Tables 2.5 and 2.6, all the three β value within the same coupled scin-

tillators are compatible, but the same cannot be said for the values between the two couples. This can be the result of systematic errors belonging to the non-ideality of the experimental setup, for example the different position of the PMT attached to every scintillator: this will produce a delay in the photon collection at the PMT level, depending on the position of the interaction between the incoming muon and the scintillator.

Additionally, and more relevant, the errors associated to this measurement consider as null the uncertainty on the distances between the four scintillators. Indeed, the way these parameters have been measured leads to errors much larger than the sensibility of the measuring tape used, and thus not negligible. Another error come from the fact that the thickness of the scintillator is not infinitesimal, but it is of few centimeters, leading to intrinsic uncertainties related to the starting and final point of the trajectory. For all these reasons it is necessary to add an error contribution to the average β of each couple (last row of Tables 2.5 and 2.6).

The contribution to the β error described so far, can be calculated according to the propagation expression:

$$\beta = \frac{H}{c \cdot ToF} \qquad \longrightarrow \qquad \sigma_\beta^H = \beta \cdot \frac{\delta H}{H} = \beta \cdot 2\%_H$$

This means that for a distance of 369cm there is an error of about 7cm, which seems reasonable considering what said before.

Adding this contribution, the final values for the two means are shown in Table 2.7:

mean β_{02}	1.027 ± 0.021
mean β_{13}	1.01 ± 0.02

Table 2.7: Mean with recalculated errors.

The final result for the velocity is estimated as the mean of these two values. Comparing it with the expected $\beta = 0.99$ for relativistic muon, we find compatibles values.

$$\beta \pm \sigma_\beta = 1.018 \pm 0.021$$

Chapter 3

Conclusion

The experiment on the muon flux allows to determine several properties of this particle. Through scintillators and digital equipment, the coincidence measurements can be easily performed. After a data rejection procedure, whose aim is to cut away the problematic ToF data, and a coherent estimation of the experimental errors involved, the final value of the total flux and the velocity of muons β can be carried out with good agreement with the expectation.

The resolution of our measurement is mainly affected by the uncertainty on the distance traveled; this error is even larger when considering also the inclination of the trajectory with respect to the perpendicular, which enlarge further the total path. Here this contribution is neglected.

An improvement of this experiment could be the alignment of the PMTs that allows to reduce the collection delay, and a more precise estimation of the distances, implementing a better measuring procedure. On the other hand, the error coming from ToF 02 and ToF 13 is negligible with respect to the one of the path, so it could be a solution reducing the distance (even though the time error would be larger) to improve the systematic error.